Journal of the Serbian Chemical Society
JSCS@tmf.bg.ac.rs • www.shd.org.rs/JSCS
J. Serb. Chem. Soc. *87* (9) 1035–1048 (2022)
JSCS–5576
Original scientific paper
Published 26 August 2022

Oxide coatings with immobilized Ce-ZSM5 as visible light photocatalysts

NIKOLA BOŽOVIĆ[1,2], KRISTINA MOJSILOVIĆ[1], SRNA STOJANOVIĆ[3#], LJILJANA DAMJANOVIĆ-VASILIĆ[3#], MARIA SERDECHNOVA[4], CARSTEN BLAWERT[4], MIKHAIL L. ZHELUDKEVICH[4,5], STEVAN STOJADINOVIĆ[1] and RASTKO VASILIĆ[1]*

[1]*University of Belgrade, Faculty of Physics, Studentski trg 12–16, 11000 Belgrade, Serbia,* [2]*Directorate of Measures and Precious Metals, Mike Alasa 14, 11000 Belgrade, Serbia,* [3]*University of Belgrade, Faculty of Physical Chemistry, Studentski trg 12–16, 11000 Belgrade, Serbia,* [4]*Institute of Surface Science, Helmholtz-Zentrum Hereon, Max-Planck--Straße 1, 21502 Geesthacht, Germany and* [5]*Institute of Materials Science, Faculty of Engineering, Kiel University, Kaiserstraße 2, 24143 Kiel, Germany*

(Received 19 May, revised 13 July, accepted 16 July 2022)

Abstract: The preparation and properties of oxide coatings with immobilized ZSM-5 zeolite obtained by plasma electrolytic oxidation on aluminum support were investigated and discussed. Pure and Ce-exchanged ZSM-5 were immobilized on aluminum supports from a silicate-based electrolyte under ultra-low duty cycle pulsed direct current conditions. The obtained composite coatings were characterized with respect to their morphology, phase and chemical composition, as well as photocatalytic activity and anti-corrosion properties. All mentioned properties of the obtained coatings were dependent on the processing time. The coatings with Ce-exchanged ZSM-5 showed higher photocatalytic activity and more effective corrosion protection than those with pure ZSM-5. The highest photocatalytic activity was observed for coatings processed for 30 min. It is suggested that the surface morphology, Ce-content and number of defects influenced the photocatalytic activity of the composite coatings.

Keywords: plasma electrolytic oxidation; zeolites; multifunctional coatings.

INTRODUCTION

Photocatalytic degradation of hazardous substances under appropriate irradiation is considered to be an advanced technology in wastewater treatment, and for that purpose many metal oxide semiconducting photocatalysts have been developed.[1–4] A large number of developed photocatalysts feature prominent

* Corresponding author. E-mail: rastko.vasilic@ff.bg.ac.rs
# Serbian Chemical Society member.
https://doi.org/10.2298/JSC211203058B

photoactivity only upon irradiation by UV light that occupies a small fraction of solar radiation, rendering visible light photocatalysis as a direction for research.[5]

Common photocatalytic processes are performed in reactors where photocatalysts are in the form of powders (particles), resulting in drawbacks such as agglomeration, obstruction of light penetration, necessity for separation from the reaction medium, *etc*.[6] To avoid these obstacles, some groups have tried to immobilize semiconducting photocatalysts on supports that could improve the overall performance of photocatalytic systems.[6–8] In the formation of such composite photocatalysts, plasma electrolytic oxidation (PEO) has proved itself to be a valuable tool for producing cost- and time-effective photocatalysts.[9] Furthermore, PEO processing enables the incorporation of electrolyte components (including particles) into coatings, providing a pathway for tailoring the properties of such composite coatings.[10–12]

Zeolites are highly porous crystalline materials, characterized by large surface area, exceptional adsorption properties and ion-exchange capacity. Their three-dimensional frameworks have well-defined structures, including pores and channels. The primary building units of the framework of zeolites are TO_4 (T = Si or Al) tetrahedra linked together by sharing oxygen atoms. The negatively charged zeolitic framework needs extra-framework charge-compensating cations, which are located in pore structure and can be easily replaced by other cations *via* ion exchange process.[13] A recent study has shown that incorporation of both natural and synthetic zeolites loaded with Ce can enhance the photocatalytic properties of PEO coatings obtained under ultra-low duty cycle conditions on an aluminum substrate.[14] However, the amount of Ce with which the synthetic zeolite 13X was loaded was rather high (about 30 wt. %), which is an obstacle for industrial applications.

Since the type, number and location of extra-framework cations strongly influence the characteristics of zeolites, in this paper the immobilization of Ce-loaded ZSM-5 zeolite into PEO coatings on aluminum is presented. ZSM-5 zeolite belongs to MFI structural type and it has a pore system formed of zigzag 10-membered ring channels (0.51 nm×0.55 nm) interconnected with other 10-membered ring channels (0.53 nm×0.56 nm) that are perpendicular to each other, the size of the channels intersection is 0.85–0.90 nm.[15] Aqueous loading of ZSM-5 with cerium is simple and requires a lower amount of cerium precursor in comparison to both 13X and clinoptilolite zeolites.[14] The composite coatings are formed by PEO processing from a silicate-based electrolyte with the addition of pure and Ce- exchanged ZSM-5 zeolites. The obtained coatings were characterized with respect to their morphology, chemical and phase composition as well as for application in photodecomposition of organic pollutants, where Methyl orange served as a model pollutant.

EXPERIMENTAL

The starting material in this work was the ammonium form of zeolite ZSM-5 (Si/Al = = 11.5) obtained from Zeolyst. The NH_4-ZSM-5 was transformed to the H-ZSM-5 ($H_{7.68}(H_2O)_{16}(Al_{7.68}Si_{88.32}O_{192})$) form by calcination at 500 °C for 5 h. Preparation of cerium containing zeolite was performed by ion exchange procedure in dilute aqueous solution: 5 g of zeolite was suspended in 1 L of 0.003 M $Ce(NO_3)_3{\cdot}6H_2O$ solution (purity 99 %, purchased from Aldrich), then stirred for 7 days at room temperature (*ca*. 21 °C), followed by filtering, rinsing with deionized water and drying overnight at 80 °C in air. This procedure was performed twice to increase the cation exchange in ZSM-5. Subsequently, the obtained zeolite was calcined at 500 °C for 5 h in air. The cerium content, determined by Energy Dispersive X-Ray Fluorescence Spectroscopy using a Thermo Scientific™ Niton™ XL3t GOLDD+ XRF Analyzer, was 1.1±0.4 wt. %.

Rectangular samples of AA1050 aluminum alloy were set as the anodes and used as the support for zeolite immobilization. A stainless steel sheet of approx. 20 cm^2 was used as cathode in all experiments. The anode material was sealed with insulation resin leaving an active surface area of approx. 2.5 cm^2 accessible to electrolyte. An aqueous solution of 4 g L^{-1} Na_2SiO_3 + 4 g L^{-1} KOH was used as the supporting electrolyte for all experiments, with additions of 1 g L^{-1} of ZSM-5 zeolite (either pure or exchanged with Ce).

The electrolytes used in this study (Table I) were prepared using double distilled and deionized water and pro analysis grade chemical compounds. The PEO process was carried out in a jacketed electrolytic cell maintaining the temperature of the electrolyte below 30 °C. During PEO processing, all electrolytes with zeolite addition were agitated by a magnetic stirrer. A home-made pulsed DC power supply working in the galvanostatic (current controlled) mode was used for this experiment. The power supply produced rectangular pulses of 2.5 A and PEO processing was performed under a current density of 1 A cm^{-2} during 10, 20, 30 and 40 min with a t_{on} of 10 ms and t_{off} of 1 s for all experiments (corresponding to *ca*. 1 Hz frequency and 1 % duty cycle).

TABLE I. Electrolytes used in this study and their designation

Sample	Electrolyte	pH	Conductivity, mS cm^{-1}
ZSM5	4g/L Na_2SiO_3+4g/L KOH +1 g/L ZSM5	12.36	13.14
ZSM5+Ce	4g/L Na_2SiO_3+4g/L KOH +1 g/L ZSM5+Ce	12.18	14.46
SE	4g/L Na_2SiO_3+4g/L KOH	12.15	12.99

A scanning electron microscope (SEM, JEOL 840A) was used to examine the surface morphology of the PEO layers. The chemical composition of the top surface of the coatings was analyzed with energy dispersive spectrometer (EDS, Oxford). The presented EDS results are the average of five different surface areas. The surface roughness of the obtained coatings were estimated from atomic force micrographs (AFM, Veeco Instrument) using NanoScope 7.0 software, while the porosity data was extracted from AFM micrographs using ImageJ software. For cross-sectional SEM analyses, the samples were embedded in epoxy resin and polished with 220, 1000 and 4000 SiC abrasive papers, followed by polishing with 1 μm diamond paste.

Rigaku Ultima IV diffractometer with Ni-filtered CuK_α radiation source was used for crystal phase identification. The crystallographic data were collected either in Bragg–Brentano geometry or in grazing incidence geometry (1° incidence angle), in the 2θ range from 10 to 70° at a scanning rate of 2° min^{-1}.

Photoluminescence (PL) spectral measurements were taken on a Horiba Jobin Yvon Fluorolog FL3-22 spectrofluorometer, with a 450 W xenon lamp as the excitation light source. The obtained spectra were corrected for the spectral response of the measuring system and the spectral distribution of the excitation light source.

The photocatalytic activity of the obtained coatings on Al substrate was determined by degrading Methyl orange (MO) at room temperature (*ca*. 21 °C). The samples were immersed into 10 mL of 8 mg L^{-1} aqueous MO solution and placed on a perforated holder with a magnetic stirrer underneath. Prior to irradiation, the solution and the catalyst were magnetically stirred in the dark for the corresponding irradiation time to check adsorption properties of the coatings. For irradiation, an Osram Vitalux lamp (300 W) that simulates solar spectrum was placed 25 cm above the top surface of the solution (corresponding to an illumination intensity of about 16000 lx). A fixed quantity of the MO solution was removed every hour to measure the absorption and then to determine concentration using a Agilent Carry 60 UV–Vis spectrophotometer. After each measurement, the probe solution was returned to the photocatalytic reactor. Prior to the photocatalysis measurements, the MO solution was tested for photolysis in the absence of the photocatalyst in order to examine its stability. The lack of change in the MO concentration after 6 h of irradiation revealed that degradation was only due to the presence of the photocatalyst. The presented photocatalysis results are averaged results of four measurements (two samples tested on both sides).

The degradation behavior of PEO treated specimens (and bare substrate for comparison) was investigated *via* electrochemical impedance spectroscopy (EIS) measurements using a Gill AC potentiostat (Gill AC, ACM Instruments, UK) in 3.5 wt. % NaCl solution (*ca*. 300 mL). A traditional three-electrode cell containing an Ag/AgCl reference electrode, platinum counter electrode and specimen as a working electrode (exposed area of 0.5 cm^2) was used. All electrochemical tests were performed under normal atmosphere at room temperature (*ca*. 21 °C) using a magnetic stirring (*ca*. 200 rpm). The EIS measurements were performed *vs*. OCP with an AC amplitude of 10 mV (RMS) over a frequency range of 30000–0.5 Hz (overall 70 data points were recorded). The impedance spectra were collected after immersion for 1, 3, 6, 12, 24, 48, 72, 96, 120, 144 and 168 h in order to study the degradation process as a function of immersion time. The presented results are averaged results for two samples (one side each).

RESULTS AND DISCUSSION

Morphology, chemical and phase composition of obtained coatings

After the PEO processing, the obtained composite coatings on aluminum substrate were first tested for their crystallinity and phase composition using X-ray diffraction (XRD). Survey XRD patterns of the coatings with immobilized zeolites obtained in the focusing (Bragg–Brentano) mode are shown in Fig. 1a.

The observed diffraction maxima were indexed to crystalline phases originating from the Al substrate, γ-alumina and aluminosilicate phase sillimanite. The XRD maxima originating from pure and Ce-exchanged ZSM-5 zeolites are not present in these diffractograms, most probably as a result of their low concentration and/or good dispersion in the obtained coatings. It can also be observed that prolonged PEO processing time results in a decrease of diffraction maxima originating from the substrate and an increase of the diffraction maxima denoted as γ+Sil (γ-Al_2O_3 + sillimanite). As in the case of clinoptilolite and 13X zeolite

used in a previous study, a more detailed inspection of diffraction maxima increasing with PEO processing time (Fig S-1 of the Supplementary material to this paper) shows that at the beginning of PEO processing this peak could be attributed to crystalline γ-alumina (JCPDS 10-0425) phase, while at later processing times. it shifts towards aluminosilicate sillimanite (JCPDS 22-0018) crystalline phase.[14]

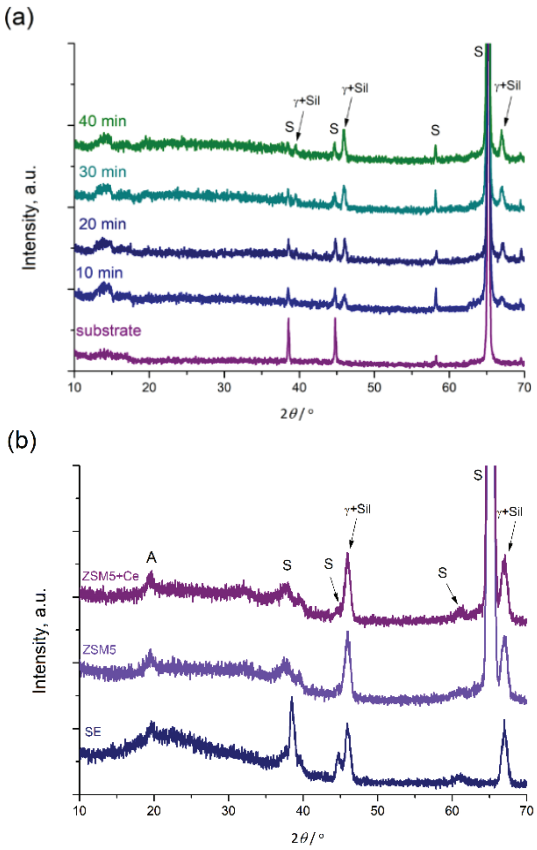

Fig. 1. a) Focusing mode XRD patterns of oxide coatings on Al containing ZSM-5 zeolites obtained for various PEO processing times; b) grazing incidence XRD patterns of oxide coatings.

For additional analysis of phase composition of obtained coatings, a grazing incidence XRD (GIXRD) measurement was performed and results are presented in Fig. 1b. X-ray diffraction under small incidence angle reveals the crystallinity of the topmost part of the oxide coating and showed the presence of another aluminosilicate crystalline phase andalusite (denoted as A). Andalusite is a low-temperature (and low-pressure) aluminosilicate phase that can be transformed to sillimanite either by increasing the temperature or by increasing the pressure.[16] Since locally high temperatures and pressures are intrinsic to PEO processing, it could be hypothesized that andalusite forms on the outer layer of the coating

when the electrolyte reach the molten oxide from micro-discharging channels.[9] With prolonged PEO processing, under high temperature and pressure, it transforms into sillimanite. Furthermore, it is well known that all aluminosilicates contain Si^{4+} atoms in four-fold coordination and Al^{3+} atoms in six-fold coordination, but sillimanite and andalusite also contain aluminum in four-fold and five-fold coordination, respectively.[17] This suggests that prolonged PEO processing introduces a number of oxygen vacancies into PEO coatings, which is an important factor governing the photoluminescent and photocatalytic properties of obtained coatings as discussed later in more detail.

The surface morphology of coatings obtained for various PEO processing times in supporting electrolyte containing 1 g/L of Ce-exchanged ZSM-5 zeolite are presented in Fig. 2. SEM micrographs show the usual cracked pancake-like morphology decorated by dispersed beads attached to the coating surface, typical of the PEO coatings on Al and its alloys.[18] Similar surface morphology was evidenced for composite coatings obtained from an electrolyte containing pure ZSM-5 (Fig. S-2 of the Supplementary material).

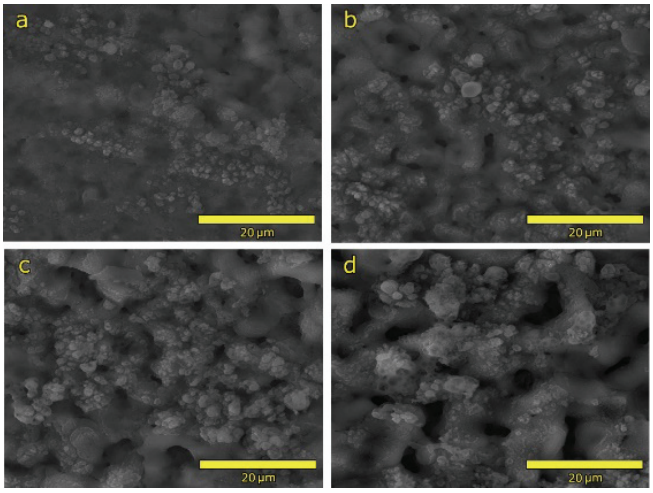

Fig. 2. Top-view micrographs of coatings obtained in 4 g L^{-1} Na_2SiO_3 + 4 g L^{-1} KOH + 1g L^{-1} ZSM-5+Ce after: a) 10, b) 20, c) 30 and d) 40 min.

To quantify the change in the surface morphology of the obtained coatings, AFM characterization was conducted (Fig. 3, and Fig. S-3 of the Supplementary material). Although roughness and porosity data can also be extracted from SEM images using appropriate free distribution software, AFM images give a much better in-depth view and usually provide more precise information about surface morphology. These results are presented in Table II.

Obviously, roughness (presented as R_a, which is the arithmetic average of the absolute values of the deviations of the profile height from the mean line, rec-

orded within the evaluation length) increases with PEO processing time for both zeolite-containing electrolytes. Data from Table II can be related to the influence of PEO processing time on the morphology of the coatings. Namely, the longer PEO processed coatings are thicker and require higher energy for each dielectric breakdown. As a result, the current is localized at defects in the oxide layer leaving behind a discharge channel of a larger diameter.[18] As observed from visual inspection of both AFM and SEM micrographs, the number of the micro-discharging channels decreases while the size of the pores observable on the surface of coating increases with PEO processing time.

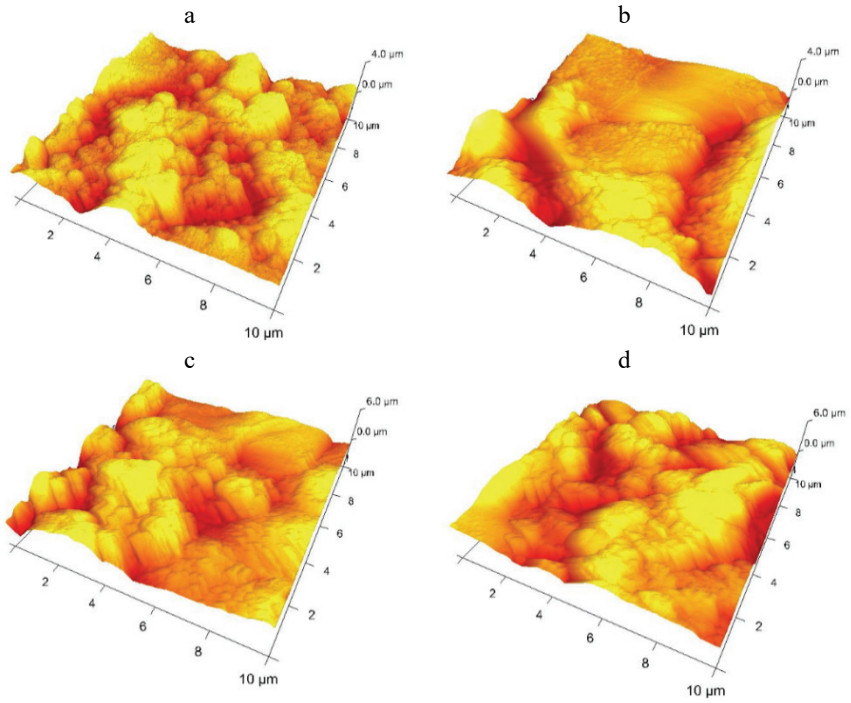

Fig. 3. Three-dimensional AFM images of oxide coatings formed in supporting electrolyte with Ce-exchanged ZSM-5 zeolite at various stages of the PEO process: a) 10, b) 20, c) 30 and d) 40 min.

The quantitative chemical composition of the surface of the prepared oxide coatings was obtained utilizing EDS measurements. EDS data (as weight percentage (wt. %)) of the elements present in the coatings is given in Table S-I of the Supplementary material. The main elements of the coatings were Al, O, Si, Na and K, indicating the contribution of elements from both substrate and electrolyte. Taking into account the accuracy of the method for chemical composition determination, it is evident from Table S-I that the contents of all elements are

very similar for all coatings. Unfortunately, as in the case of composite coatings with Ce-exchanged zeolites from tungstate electrolyte, Ce was not quantitatively detected, which may be caused by its small concentration in Ce-loaded zeolites, *i.e.*, as already stated, the estimated amount of Ce in ZSM-5 zeolite was about 1.1 wt. %, which is far below its concentration in the previously used clinoptilolite and 13X zeolites.[13,19] Representative cross-sections of the oxide coatings formed after different PEO processing periods are shown in Fig. S-4 of the Supplementary material. As observable, the obtained coatings are continuous showing well developed porosity and roughness, as outlined in Table II. Coating thickening and compaction are the result of addition of zeolite particles to the supporting electrolyte and their probable stimulated reactive incorporation into the oxide coatings due to the low melting point.[10] The presence of whiter regions in all the cross sections in Fig. S-4 could be observed, suggesting either an increased concentration of Ce or incorporation of zeolite particles into the coatings. Unfortunately, EDS analyses could not confirm an increased Ce content due to its low concentration, while incorporation of zeolite particles was not confirmed because their chemical composition is identical to the chemical composition of oxides originating from the substrate and electrolyte.

TABLE II. Surface roughness and porosity data for the obtained coatings (experimental error is calculated as standard deviation for five measurements)

Sample	PEO time, min	R_a / nm	Porosity, %
ZSM5	10	410±85	24±2
	20	458±105	20±2
	30	587±68	18±1
	40	688±21	14±1
ZSM5+Ce	10	426±82	20±2
	20	461±87	16±1
	30	601±21	14±1
	40	747±46	11±1

A set of luminescence measurements was performed in order to qualitatively probe the amount of Ce, because it is well known that Ce^{3+} doped Al_2O_3 PEO coatings exhibit an intense PL emission in the ultraviolet/visible spectral range with PL maximum positioned around 345 nm under 285 nm excitation due to the transitions of Ce^{3+} from the 5d excited state to the 4f ground state.[20] Emission PL spectra of PEO coatings obtained in an electrolyte containing 1 g L^{-1} of ZSM5+Ce are presented in Fig. 4. The PL spectra observed for coatings containing Ce-exchanged ZSM-5 zeolite are composed of two spectral maxima. The first sharp maximum was positioned at about 345 nm, while the other one is broad and is centered at about 440 nm. Based on previous results, it is clear that the broad maximum centered at about 440 nm is related to Al_2O_3 photoluminescence originating from optical transitions in PL centers that are defect centers related to

oxygen vacancy defects in Al_2O_3 PEO coatings (F and F^+ centers).[21] This finding is also in agreement with high resolution XRD patterns showing that coatings obtained using shorter PEO treatment times contain almost exclusively crystalline γ-Al_2O_3 phase (Fig. S-1). Since the PL intensity of Ce^{3+} doped Al_2O_3 coatings depends on the PEO processing time and the concentration of Ce-species in the electrolyte, *i.e.*, it entirely depends on content of Ce^{3+} incorporated into the PEO coatings, it could be concluded that Ce is present in all coatings (with Ce concentration increasing with PEO time) but quantification was not possible because of its low content.[19] Furthermore, from Fig. 4 it could be observed that the PL intensity of the broad 440 nm emission peak increases with PEO processing time, thus suggesting that the number of oxygen vacancy related defects increases with PEO processing time. This is also in line with the observed phase transformation from andalusite to sillimanite (Fig. 1b), which introduces oxygen vacancies.[17]

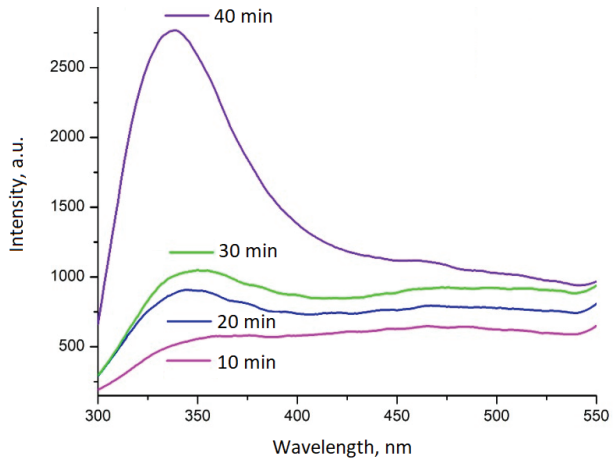

Fig. 4. Emission PL spectra of the obtained coatings under 285 nm excitation.

Photocatalytic activity of the obtained coatings

Photocatalytic activity of Methyl Orange photodegradation is presented in Fig. 5 for all obtained coatings. If the irradiation light photon energy is higher than the band-gap energy of a semiconducting photocatalyst it results in the excitation of electrons from the valance band to the conduction band, thus generating electron–hole pairs. Photogenerated electrons and holes participate in oxidation and reduction reactions with water and dissolved oxygen to form hydroxyl radicals and superoxide radicals, which possess high redox activity and participate in reactions with an adsorbed substance. Photoactivity is always hindered by the recombination of photogenerated electron-hole pairs.[6] The best photocat-

alytic activity was observed for the coating obtained after 30 min of PEO processing in supporting electrolyte with addition of 1 g L^{-1} of ZSM-5+Ce zeolite.

In fact, it could be observed that for all coatings the photocatalytic activity increases with PEO treatment time up to 30 min, after which it levels off or even decreases. Based on the surface morphology data extracted from the AFM micrographs, it could be speculated that the photoactivity is influenced by an interplay between the surface roughness and porosity: since roughness increases while the porosity decreases with PEO processing time, larger, irregularly shaped pores may prevent light, as an immaterial agent, from penetrating towards the active centers positioned deeper inside the composite coatings, leaving only centers close to the surface accessible for photodecomposition of MO. Clearly, Fig. 5 shows that when Ce-exchanged ZSM-5 zeolite is incorporated into oxide coatings, the photoactivity of the obtained coatings increases almost linearly, compared to coatings without Ce.

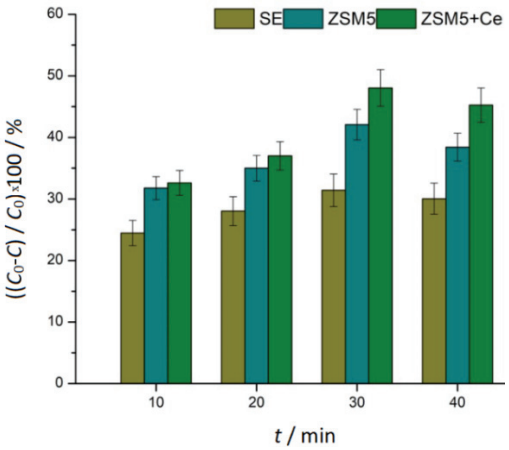

Fig. 5. Photocatalytic degradation of MO on composite zeolite coatings.

Therefore, the Ce-content could be excluded as the reason for the observed photoactivity decrease. It is also well known that oxygen vacancy defects play an important role in photoactivity of metal oxide photocatalysts.[22,23] XRD data (Fig. 1) shows that prolonged PEO processing time results in the formation of an aluminosilicate phase that possesses a high density of oxygen vacancies, which was also confirmed by PL measurements (Fig. 4). Bearing all this in mind, it could be suggested that the observed decrease in photoactivity is solely related to morphology of the coatings.

Degradation stability of the obtained coatings

Given the liquid environment in which photocatalytical decomposition of organic pollutants usually occurs, degradation stability tests of the coatings were performed utilizing EIS (Fig. 6). The obtained results demonstrate certain scatter-

ing at low frequencies, which is often attributed to active-passive transitions in the case of PEO coated substrates. The activation of a defect during the recording of the impedance spectra causes a drop of the low frequency impedance values and could cause a shift of the OCP and as a consequence, non-stationary behavior during recording of the data. Due to this fact, a detailed analysis of the EIS data was not performed. Nevertheless, it is obvious that incorporation of pure ZSM-5 zeolite decreases the corrosion resistance of the coatings (see the data for bare substrate and substrate with PEO coating formed in supporting electrolyte[14]). This is most likely by adding more defects to the coatings by the incorporated particles.

Although it was not possible to quantify the cerium content in EDS, it was demonstrated by PL measurements, as well as by the increased photocatalytic activity, that Ce is present in the composite coatings when Ce loaded ZSM-5 zeolite was used in PEO processing and that the Ce content increased with treatment time.

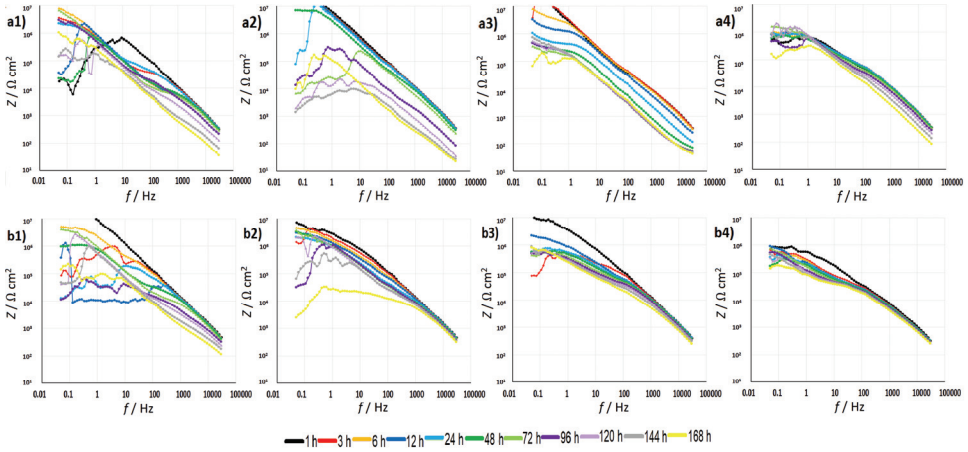

Fig. 6. Representative EIS results for the obtained zeolite-containing composite coatings: a) coatings formed in electrolyte containing ZSM-5 zeolite processed for: 10 (a1), 20 (a2), 30 (a3) and 40 min (a4); coatings formed in electrolyte containing ZSM-5+Ce zeolite processed for: 10 (b1), 20 (b2), 30 (b3) and 40 min (b4).

A similar positive trend due to the Ce addition was also visible for the corrosion resistance. It is obvious that the deep drops of the low frequency impedance are somewhat less pronounced for the Ce-containing systems (for the same immersion times) evidencing the easier passivation of the formed defects. Comparing the evolution of impedance modulus curves for ZSM-5 zeolite containing PEO coatings with and without Ce, an important difference could be observed, namely a higher stability of the impedance modulus values at high to middle frequencies for Ce-loaded systems, where the response from the barrier layer was

evidenced. This effect might be attributed to an active stabilization of this layer by Ce-based species released form the zeolite particles.[24]

CONCLUSIONS

Composite oxide coatings with immobilized pure and Ce-exchanged ZSM-5 zeolite were deposited on aluminum support from silicate-based electrolyte using PEO processing. All the coatings were partially crystallized containing γ-alumina and the aluminosilicate phase sillimanite. GIXRD shows that the aluminosilicate phase andalusite was present in the outer layer of the coatings. The surface morphology of the obtained coatings depends on the PEO processing time. The roughness of the obtained composite coatings increased with PEO time, but their porosity decreased. The coatings contained elements originating from the substrate and from the electrolyte. The cerium concentration was below the detection limit of EDS in coatings formed from electrolyte that contains Ce-loaded ZSM-5 zeolite. PL was utilized as a tool to qualitatively probe the Ce content in the coatings and showed that it increased with prolonged PEO processing time.

The highest photocatalytic activity was observed for coatings with immobilized Ce-exchanged ZSM-5 zeolite processed for 30 min. Coatings containing Ce-exchanged ZSM-5 zeolite show higher photoactivity than those with immobilized pure ZSM-5 zeolite. The effect of Ce on the anti-corrosion properties was not very strongly pronounced due to its low concentration in the coatings but it was still visible. Corrosion observations suggested that the coatings containing Ce had a higher corrosion resistance.

Acknowledgements. This work is supported by the Ministry of Education, Science and Technological Development of the Republic of Serbia, contract numbers: 451-03-68/2022--14/200162 and 451-03-68/2022-14/200146), and by the European Union Horizon 2020 research and innovation program under the Marie Sklodowska-Curie grant agreement No. 823942 (FUNCOAT).

ИЗВОД

ФОТОКАТАЛИТИЧКИ ОКСИДНИ СЛОЈЕВИ СА ИМОБИЛИСАНИМ Ce-ZSM5 ЗЕОЛИТОМ

НИКОЛА БОЖОВИЋ[1,2], КРИСТИНА МОЈСИЛОВИЋ[1], СРНА СТОЈАНОВИЋ[3], ЉИЉАНА ДАМЈАНОВИЋ-ВАСИЛИЋ[3], MARIA SERDECHNOVA[4], CARSTEN BLAWERT[4], MIKHAIL L. ZHELUDKEVICH[4,5], СТЕВАН СТОЈАДИНОВИЋ[1] и РАСТКО ВАСИЛИЋ[1]

[1]Универзитет у Београду, Физички факултет, Студентски трг 12–16, 11000 Београд, [2]Дирекција за мере и драгоцене метале, Мике Аласа 14, 11000 Београд, [3]Универзитет у Београду, Факултет за физичку хемију, Студентски трг 12–16, 11000 Београд, [4]Institute of Surface Science, Helmholtz-Zentrum Hereon, Max-Planck-Straße 1, 21502 Geesthacht, Germany и [5]Institute of Materials Science, Faculty of Engineering, Kiel University, Kaiserstraße 2, 24143 Kiel, Germany

У овом раду су представљени начин припреме и особине композитних оксидних слојева са имобилисаним зеолитом ZSM-5 добијених методом плазмене електролитичке оксидације (PEO). Полазни зеолит ZSM-5 зеолит и ZSM-5 зеолит јонски измењен са Ce су имобилисани у оксидни слој на алуминијумском носачу из силикатног електролита у

условима ултра-ниског електричног оптерећења. Испитани су морфологија, фазне и хемијске особине, фотокаталитичка активност и деградација добијених композитних слојева. Показано је да све наведене особине добијених слојева зависе од времена третмана узорка. Оксидни слојеви са уграђеним ZSM-5 зеолитом јонски измењеним са Ce су показали повећану фотокаталитичку активност у односу на оксидне слојеве са имобилисаним полазним ZSM-5 зеолитом. Највећа фотокаталитичка активност је добијена за слојеве добијене после 30 min PEO третмана. Показано је да морфологија површине, количина Ce и дефекти настали у оксидним слојевима у току PEO третмана утичу на фотокаталитичку активност на овај начин добијених композитних слојева.

(Примљено. 19. маја, ревидирано 13. јула, прихваћено 16. јула 2022)

REFERENCES

1. Q. Wang, K. Domen, *Chem. Rev.* **120** (2020) 919 (https://dx.doi.org/10.1021/acs.chemrev.9b00201)
2. S. Asadzadeh-Khaneghah, A. Habibi-Yangjeh, *J. Clean. Prod.* **276** (2020) 124319 (https://dx.doi.org/10.1016/j.jclepro.2020.124319)
3. Y. Guo, M. Wen, G. Li, T. An, *Appl. Catal., B* **281** (2021) 119447 (https://dx.doi.org/10.1016/j.apcatb.2020.119447)
4. D. Ayodhya, G. Veerabhadram, *Mater. Today Energy* **9** (2018) 83 (https://dx.doi.org/10.1016/j.mtener.2018.05.007)
5. A. B. Djurišić, Y. He, A. M. C. Ng, *APL Mater.* **8** (2020) 030903 (https://doi.org/10.1063/1.5140497)
6. G. Hu, J. Yang, X. Duan, R. Farnood, C. Yang, J. Yang, W. Liu, Q. Liu, *Chem. Eng. J.* **417** (2021) 129209 (https://doi.org/10.1016/j.cej.2021.129209)
7. N. Tadić, S. Stojadinović, N. Radić, B. Grbić, R. Vasilić, *Surf. Coat. Technol.* **305** (2016) (http://dx.doi.org/10.1016/j.surfcoat.2016.08.045)
8. N. Diban, A. Pacula, I. Kumakiri, C. Barquin, M. J. Rivero, A. Urtiaga, I. Ortiz, *Catalysts* **11** (2021) 1367 (https://dx.doi.org/10.3390/catal11111367)
9. M. Kaseem, S. Fatimah, N. Nashrah, Y. G. Ko, *Prog. Mater. Sci.* **117** (2021) 100735 (https://dx.doi.org/10.1016/j.pmatsci.2020.100735)
10. X. Lu, C. Blawert, M. L. Zheludkevich, K. U. Kainer, *Corros. Sci.* **101** (2015) 201 (https://dx.doi.org/10.1016/j.corsci.2015.09.016)
11. S. Stojadinović, N. Tadić, N. Radić, B. Stojadinović, B. Grbić, R. Vasilić, *Surf. Coat. Technol.* **276** (2015) 573 (https://dx.doi.org/10.1016/j.surfcoat.2015.06.013)
12. M. Schneider, K. Kremmer, D. Tabatabai, W. Furbeth, *Mater. Corros.* **2018** (2018) 1 (https://dx.doi.org/10.1002/maco.201709969)
13. D. W. Breck, *Zeolite Molecular Sieves*, Wiley, New York, 1974, ISBN 9780471099857
14. K. Mojsilović, N. Božović, S. Stojanović, Lj. Damjanović-Vasilić, M. Serdechnova, C. Blawert, M. L. Zheludkevich, S. Stojadinović, R. Vasilić, *Surf. Interfaces* **26** (2021) 101307 (https://dx.doi.org/10.1016/j.surfin.2021.101307)
15. Ch. Baerlocher, L. B. McCusker, D. H. Olson, *Atlas of Zeolite Framework Types*, 6th rev. ed., Elsevier, Amsterdam, 2007 (https://doi.org/10.1016/B978-044453064-6/50186-9)
16. R. C. Bradt, in *Ceramic and Glass Materials*, J. F. Shackelford, R. H. Doremus, Eds., Springer, Boston, MA, 2008, p. 41 (https://doi.org/10.1007/978-0-387-73362-3_3)
17. A.D. Fortes, *Phys. Chem. Miner.* **46** (2019) 687 (https://doi.org/10.1007/s00269-019-01031-3)
18. R. Hussein, X. Nie, D. Northwood, *Surf. Coat. Technol.* **205** (2010) 1659 (https://doi.org/10.1016/j.surfcoat.2010.08.059)

19. K. Mojsilović, U. Lačnjevac, S. Stojanović, Lj. Damjanović-Vasilić, S. Stojadinović, R. Vasilić, *Metals* **11** (2021) 1241 (https://doi.org/10.3390/met11081241)
20. S. Stojadinović, R. Vasilić, *J. Lumin.* **203** (2018) 576 (https://doi.org/10.1016/j.jlumin.2018.07.008)
21. S. Stojadinović, R. Vasilić, Z. Nedić, B. Kasalica, I. Belča, Lj Zeković, *Thin Solid Films* **519** (2011) 3516 (https://doi.org/10.1016/j.tsf.2011.01.188)
22. F. Gunkel, D. V. Christensen, Y. Z. Chen, N. Pryds, *Appl. Phys. Lett.* **116** (2020) 120505 (https://doi.org/10.1063/1.5143309)
23. Z. Wang, R. Lin, Y. Huo, H, Li, L. Wang, *Adv. Funct. Mater.* **32** (2022) 2109503 (https://doi.org/10.1002/adfm.202109503)
24. S. A. S. Dias, A. Marques, S. V. Lamaka, A. Simoes, T. C. Diamantino, M. G. S. Ferreira, *Electrochim. Acta* **112** (2013) 549 (https://doi.org/10.1016/j.electacta.2013.09.026).